Analysis and Mitigation of Neutral Line Current Ripple in a Dual 3L-NPC Converter System for Bipolar DC Distribution

Bowei Li, *Graduate Student Member, IEEE*, Gregory J. Kish, *Senior Member, IEEE*, and Yunwei Li, *Fellow, IEEE*

***Abstract*—Bipolar dc distribution systems based on a three-level neutral point clamped (3L-NPC) converter typically require a voltage balancer (VB) to achieve full bipolar dc voltage balancing. Recent studies have shown that certain grid transformer configurations allow the full control of dc-side pole power flows by multitasking the converter-side windings to carry the required dc balancing current through a dedicated neutral line (NL). NL-based NPC converter systems offer a simpler and more cost-effective alternative to VB-based systems, but suffer from significant NL current ripple caused by the pulsewidth modulation (PWM) switching of the converter. This article addresses the issue on two fronts. First, an in-depth analysis of the NL current ripple is conducted in a dual NPC converter system. Analytical expressions are derived to characterize the harmonic distribution under both phase disposition (PD) and alternate phase opposition disposition (APOD) PWM strategies. Second, based on the analysis, an improved PD-PWM strategy incorporating triple degrees-of-freedom (PD-TDoF) is proposed for dual NPC converters, effectively reducing current ripple and significantly enhancing NL current performance compared to conventional PD-PWM. The theoretical analysis and effectiveness of the proposed PD-TDoF strategy are validated through laboratory experiments.**

***Index Terms*—Bipolar dc distribution, current ripple, harmonic analysis, neutral line (NL), pulsewidth modulation (PWM), three-level neutral point clamped (3L-NPC) converter.**

I. Introduction

DC distribution systems are undergoing rapid advancements at both medium voltage (MV) [1] and low voltage (LV) [2] levels, driven by their advantages of simplified renewable integration, reduced conversion stages, elimination of reactive power, and better compatibility with the increasing penetration of dc loads [3], [4], [5]. Between the two dc distribution bus structures, the bipolar configuration is considered more promising than the unipolar one, owing to its higher voltage flexibility (more voltage levels), improved reliability, and better fault management [6].

Distribution converters are a crucial component of bipolar dc distribution systems. The three-level neutral point clamped converter (3L-NPC) offers specific advantages over the two-level voltage source converter (2L-VSC), including improved output voltage quality, lower voltage stress on switches, and higher efficiency [7]. Compared to modular multilevel converters (MMC), the simpler structure and lower cost of 3L-NPC converters make them more suitable for distribution-level systems. These advantages highlight the potential of the 3L-NPC for bipolar dc distribution and motivate its adoption in practical projects, such as the ANGLE-DC project [8].

As the first MV bipolar dc distribution demonstration project in the U.K. [9], ANGLE-DC employs a multiwinding transformer and six cascaded 3L-NPC submodules for both the positive and negative poles of the $\pm$ 27 kV bipolar dc bus. This design enables independent control of each pole, ensuring voltage balance under different dc load conditions. However, this bipolar system essentially comprises two unipolar systems, which, although straightforward, leads to increases in system cost and volume. To ensure the bipolar operation capability while avoiding the drawbacks of cascaded 3L-NPC converter systems, many improved 3L-NPC-based bipolar dc distribution schemes have been proposed. Since a single 3L-NPC converter has been demonstrated to possess inherent but limited bipolar voltage balancing capability [10], [11], a common approach is adding extra circuits to maintain dc pole voltage balance under various load conditions. Such auxiliary balancing circuits, often referred to as voltage balancers (VB) [12], have been extensively studied based on existing dc–dc converter topologies [13], [14], [15]. For instance, an additional 3L-NPC leg can be employed as the VB for the 3L-NPC converter [10], as illustrated in Fig. 1(a).

Proper handling of the dc-side neutral balancing current is critical for addressing bipolar voltage imbalance. Instead of employing extra balancing devices, an alternative approach is to regulate the balancing current by creating an additional current path between the ac and dc sides. This can be done by multitasking the converter-side windings of the grid-interfacing transformer. The main concern with this method is the potential transformer core saturation caused by the zero-sequence currents in the windings. However, this issue can be prevented by

Received 15 April 2025; revised 4 August 2025; accepted 8 September 2025. Date of publication 12 September 2025; date of current version 23 December 2025. Recommended for publication by Associate Editor K. Sun. *(Corresponding author: Bowei Li.)*

The authors are with the Department of Electrical and Computer Engineering, University of Alberta, Edmonton, AB T6G 2R3, Canada (e-mail: bli4@ualberta.ca; gkish@ualberta.ca; yunwei.li@ualberta.ca).

Color versions of one or more figures in this article are available at https://doi.org/10.1109/TPEL.2025.3609810.

Digital Object Identifier 10.1109/TPEL.2025.3609810

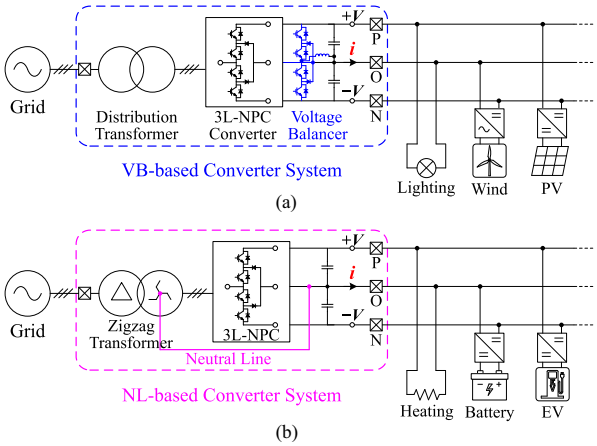

Fig. 1. Exemplars of 3L-NPC converter systems used for bipolar DC distribution. (a) VB-based. (b) NL-based.

specific winding arrangements that achieve dc flux cancellation in the core, e.g., zigzag or center-tapped windings. To elucidate, Fig. 1(b) [11] illustrates a dedicated neutral line (NL) connected between the midpoint of dc-link capacitors and the neutral point of a zigzag transformer, which can draw or inject the required dc-side neutral balancing current under proper control strategies without risk of core saturation. Moreover, there is no penalty of increased component ratings imposed with this approach [11], [16]

The absence of additional switches and the resulting lower cost represent a key advantage of NL-based NPC converter systems over VB-based systems. However, the dedicated NL linking the ac and dc sides may introduce power quality challenges to dc distribution systems. As will be demonstrated in Section II, significant ripple occurs in the NL current, leading to adverse effects and necessitating effective mitigation.

The neutral wire ripple is a well-known issue in traditional three-phase four-wire (3P4W) ac distribution systems. Its causes, composition, and adverse effects have been extensively studied and are reviewed in Section II for comparison. However, in NL-based bipolar dc distribution systems, the NL current ripple problem has not been studied effectively. The NL current is composed of zero-sequence components related to dc loads and distribution converters, but the precise mechanisms underlying current ripple formation in 3L-NPC converter systems are not yet fully understood. In particular, zero-sequence harmonic components are influenced by different pulsewidth modulation (PWM) strategies, such as phase disposition (PD) and alternative phase opposite disposition (APOD), which are two common carrier-based PWM techniques for 3L-NPC converters. In PD-PWM, all carriers are in phase across all bands, and thus the zero-sequence harmonics are clustered at the carrier frequency and its multiples. In contrast, APOD-PWM employs carriers in alternating opposite disposition, effectively redistributing the zero-sequence harmonics [17]. Therefore, the composition of the NL current ripple under these modulation strategies requires in-depth investigation.

Effective and economical current ripple mitigation techniques are essential for the long-term stable operation of power distribution systems. In 3P4W ac distribution systems, passive harmonic filters [18] and special transformer structures (e.g., zigzag transformers [19]) are commonly employed for neutral current compensation. While these bulky passive devices significantly reduce neutral current ripple, they can not eliminate it entirely. Custom-designed 3P4W active power filters (APFs) [20], [21] can achieve complete ripple elimination but at the expense of higher costs due to large-rating converters and increased complexity in active control methods. A hybrid approach leverages the benefits of both passive and active techniques by integrating a special transformer with a single-phase APF, such as the hybrid neutral harmonic suppressor [22]. For NL-based dc distribution systems, however, the nature of current ripple differs. The NL current ripple contains significant high-order harmonic components generated by the switching action of distribution converters, with frequencies exceeding the bandwidth of active control methods. Compared to the aforementioned traditional ripple mitigation techniques, modulation-based approaches offer a more economical alternative by eliminating the need for additional hardware. Moreover, advanced modulation techniques have shown great potential in suppressing current ripple by effectively reducing zero-sequence high-order harmonics. For instance, various modulation strategies, such as interleaved modulation [23], interleaved carrier phase-shift PWM [24], double-reference PWM [25], and integrated modulation [26], [27], have been demonstrated to reduce zero-sequence circulating current in parallel converters. However, NL-based dc distribution systems differ fundamentally from parallel converters due to the presence of dedicated transformers and the NL itself, highlighting the need for suitably designed modulation strategies to mitigate NL current ripple.

To bridge the existing research gap, this article first conducts a detailed analysis of the NL current ripple using a dual NPC converter system. The composition of NL current ripple under both PD-PWM and APOD-PWM strategies is clarified by switching harmonic analysis. To mitigate the significant NL current ripple under PD-PWM, an improved PD-PWM strategy is developed based on triple degrees-of-freedom (TDoF). By leveraging TDoF provided by carrier phase-shifting, interleaving strategies, and differential modulating signals, the proposed PD-TDoF strategy drives switching harmonics out of phase between the dual converters, thus enabling cancellation of most ripple components and an improved NL current performance compared to conventional PD-PWM. Unlike traditional ripple mitigation techniques (e.g., passive or APFs), PD-TDoF offers a more economical alternative by enabling flexible and hardware-free ripple mitigation. The contribution of this article is twofold.

1) A comprehensive switching harmonic analysis of the NL current ripple is conducted for a dual NPC converter system, revealing distinct harmonic patterns under different modulation strategies. Analytical expressions are derived to explain the formation of significant ripple under PD-PWM and the ripple cancellation under APOD-PWM.
2) A novel PD-TDoF modulation strategy is proposed for active NL current ripple mitigation. Compared to conventional PD-PWM, the proposed PD-TDoF strategy enables effective switching harmonic elimination by exploiting

TABLE I
COMPONENTS AND CAUSES OF NEUTRAL CURRENTS IN AC AND DC DISTRIBUTION SYSTEMS

Distribution system	Component	Cause
Three-phase four-wire distribution system	Fundamental	Unbalanced ac loads
	Harmonics	Nonlinear ac loads
NL-based bipolar dc distribution system	Direct-current	Unbalanced dc loads
	Harmonics	Distribution converters

three degrees of modulation freedom, achieving substantial NL current ripple reduction.

II. NL Current Ripple Problem in NL-Based NPC Converter Systems

This section first reviews neutral currents in both ac and dc distribution systems, highlighting their differences in composition. An NL-based dual NPC converter system is then introduced as the study platform, followed by a demonstration of the NL current ripple issue through simulations.

A. Neutral Currents in AC and DC Distribution Systems

In traditional ac distribution, 3P4W systems are more common than the three-phase three-wire ones due to their unmatched capability to supply mixed loads. The additional neutral wire provides a return path for zero-sequence currents, ensuring stable voltages in the presence of single-phase loads or unbalanced three-phase loads. However, the current flowing in the neutral conductor (i.e., neutral current) is particularly susceptible to overload and distortion, given the widespread load imbalance and nonlinear loads [19]. The neutral current typically comprises two parts: 1) a zero-sequence fundamental component caused by unbalanced loads, and 2) zero-sequence harmonic components resulting from nonlinear loads [22].

In bipolar dc distribution, the two-pole three-wire structure resembles three-phase ac systems, with the added NL in Fig. 1(b) functioning analogously to a fourth wire. The NL between ac and dc sides serves as a path for the dc-side balancing current, maintaining pole voltage balance under dc load imbalance conditions. However, similar to 3P4W systems, the NL current also suffers harmonic distortion. This distortion stems from distribution converters, which act as nonlinear loads due to semiconductor device characteristics and switching mechanisms. The NL current is also composed of two parts: 1) a beneficial dc component used for the dc-side balancing under the asymmetrical loads, and 2) undesirable zero-sequence harmonic components resulting in the NL current ripple problem.

Based on the above, the neutral current components and their causes in both systems are compared in Table I.

In 3P4W systems, large neutral current ripple may result in excessive power losses, overheating, and even failure of the neutral conductor, while also degrading power quality and risking the saturation of distribution transformers [19]. Along with the significant NL current ripple, these adverse effects are also observed in NL-based dc distribution systems. Similar to practices and methods used in traditional ac distribution systems [28], [29], [30], several temporary measures can be adopted to mitigate these effects, such as oversizing the NL or adding an additional NL. However, while partially effective, these measures come with high costs and may compromise overall system performance. Therefore, the implementation of effective ripple mitigation methods is regarded as the most promising solution for managing the NL current ripple issue.

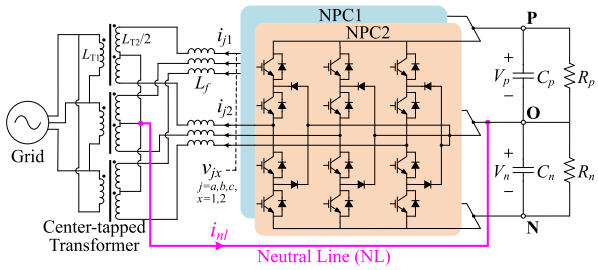

Fig. 2. Structure of the NL-based dual NPC converter system.

B. NL-Based Dual NPC Converter System

To further analyze the NL current ripple issue in bipolar dc distribution systems, an NL-based NPC converter system is introduced as the study platform. Fig. 2 depicts a dual NPC converter system [31] for high-power bipolar dc distribution. A center-tapped transformer is adopted to enable power transmission by regulating the positive-sequence currents, while preventing core saturation through precise control of the zero-sequence currents. An NL is connected between the center taps of the transformer windings and the dc-side neutral terminal, providing a path for dc-side balancing currents. Through the differential operation of the dual converters, this system can maintain bipolar dc voltage balance under completely unbalanced load conditions and improve dc-side power quality by reducing voltage and current ripple in the poles.

Despite these advantages, the dual NPC converter system is still subject to the NL current ripple issue, which will be explained and demonstrated in the following discussion.

C. Demonstration of the NL Current Ripple Issue

In NL-based bipolar dc distribution systems, three-phase currents consist of both positive-sequence (differential-mode, DM) and zero-sequence (common-mode, CM) components. The NL current is the algebraic sum of three-phase currents, and thus only contains CM components. To analyze the high-frequency components of NL current ripple in Fig. 2, a $\Sigma\Delta$-domain circuit is presented in Fig. 3, where phase a voltages and currents of NPC1 and NPC2 are decomposed into CM (Σ) and DM (Δ) components. L_f denotes the filter inductance, and L_{T2} represents the transformer's secondary winding inductance.

In the dual NPC converter system, the CM voltage of the xth ($x = 1, 2$) converter is calculated as

$$v_{\Sigma x} = \frac{1}{3}\left(v_{ax} + v_{bx} + v_{cx}\right). \tag{1}$$

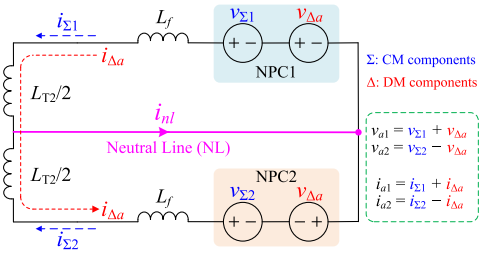

Fig. 3. ΣΔ-domain circuit for the NL current ripple analysis.

TABLE II
SIMULATION PARAMETERS FOR THE DUAL NPC CONVERTER SYSTEM

Parameter	Value	Parameter	Value
Grid RMS line voltage	36 kV	DC-link voltage	20 kV
Grid frequency	50 Hz	Switching frequency	5 kHz
Transformer turns ratio	$3\sqrt{3}:1:1$	Capacitance per pole	2 mF
Filter inductance (L_f)	8 mH	DC loads (R_p, R_n)	20 Ω

According to Fig. 3, the CM current of the xth converter is calculated as

$$i_{\Sigma x} = \frac{v_{\Sigma x}}{Z_\Sigma} = \frac{v_{\Sigma x}}{\omega(L_f + L_{T2}/2)}. \tag{2}$$

Note that only harmonic components of $i_{\Sigma x}$ are considered here, while the dc component is determined by the requirements for dc-side voltage balancing.

Finally, the NL current ripple is expressed as the sum of the CM currents from NPC1 and NPC2

$$i_{nl} = 3i_{\Sigma 1} + 3i_{\Sigma 2}. \tag{3}$$

To illustrate the NL current ripple challenge, simulations of the dual NPC converter system in Fig. 2 are performed using the parameters in Table II.

The simulated NL current waveform and its magnified ripple profile are presented in Fig. 4. At $t = 0.2$ s, the negative load is disconnected, leading to fully unbalanced dc loads. Consequently, a dc component of -830.4 A appears in the NL current to maintain bipolar voltage balance. Significant current ripple persists under both balanced and unbalanced load conditions. The peak-to-peak ripple reaches 208.5 A, corresponding to 0.417 p.u. with respect to the dc load current ($I_{dc} = V_{dc}/2R_p = 500$ A). This indicates that the ripple amplitude is approximately 41.7% of the dc baseline, highlighting the necessity of effective ripple mitigation.

To analyze the harmonic composition of the NL current ripple, fast Fourier transform (FFT) is performed on the shaded regions of the i_{nl} waveform. As shown in Fig. 4, high-order switching harmonics dominate the NL current ripple, while low-order harmonics (e.g., 6th, 12th) exhibit negligible amplitudes and can thus be ignored. This is because odd triple-n harmonics (e.g., 3rd, 9th) are inherently eliminated by the differential operation of NPC1 and NPC2 [31]. It should be noted that these results are obtained under the PD-PWM strategy, whereas the APOD-PWM strategy may produce a different harmonic distribution. Therefore, the next section investigates the high-order harmonic distribution under both PD-PWM and APOD-PWM to clarify the ripple formation mechanisms in the dual NPC converter system.

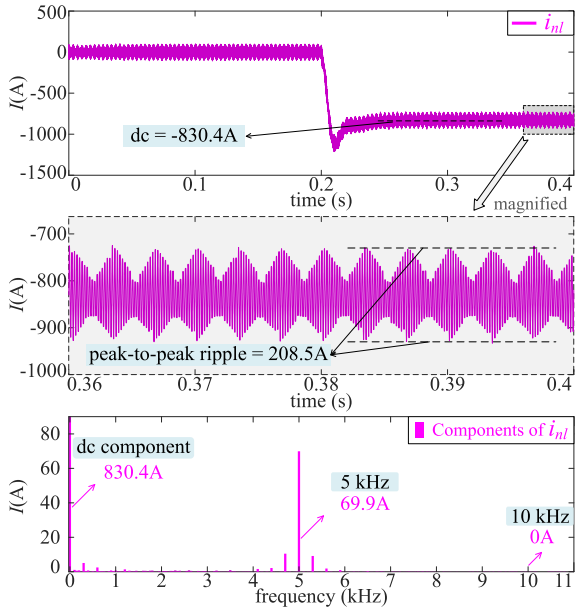

Fig. 4. Simulation waveforms of the NL current and its FFT spectrum.

III. HIGH-ORDER SWITCHING HARMONICS ANALYSIS

As an inherent nature of the power electronic converter switching, undesirable harmonics are generated as a result of the nonlinearity of loads, semiconductor switches or modulation process [17]. A well-known analytical method for determining the harmonic frequency components of PWM-switched converter systems is the double Fourier series analysis (DFSA) [32], [33]. In this method, any switched waveform of a converter can be expressed as a time-varying function in the form of a double variable controlled Fourier series, representing a summation of harmonic components. For ease of expression, a harmonic component at the frequency $(mf_c + nf_0)$ is denoted as (m, n), where m is the index of carrier frequency (f_c or ω_c), n is the index of fundamental frequency (f_0 or ω_0). For example, the fundamental component is expressed as $(0, 1)$, while $(1, 0)$ represents the harmonic component at the first carrier frequency.

Although the DFSA method has been applied to analyze the switching harmonics of parallel converters in previous studies, the dual NPC converters in Fig. 2 do not simply operate in a parallel mode due to the presence of a center-tapped transformer. The differential operation of the dual converters alters the harmonic distribution pattern and introduces new characteristics to the NL current ripple. The following subsections aim to theoretically analyze the NL current ripple under different modulation strategies, with the objective of deriving closed-form expressions that can explain practical ripple issues in the converter system. Following each theoretical analysis, simulation results are presented in parallel to verify the accuracy of the derived expressions and to illustrate the practical significance of the theoretical findings. It is known that neutral point voltage imbalance can increase current ripple in 3L-NPC converters [34]. However, the

capacitor voltage deviation in Fig. 2 is effectively suppressed by the designed control strategy even under extreme dc load imbalance [31]. Thus, the following ripple analysis is conducted under the assumption of balanced capacitor voltages, which allows focusing on the modulation impact without interference from voltage imbalance.

A. Harmonic Distribution Analysis of the NL Current Ripple Under the PD-PWM Strategy

For a PWM-switched converter, the phase voltage is composed of fundamental and harmonic components. By employing the DFSA method, the time-varying phase j ($j = a, b, c$) voltage of a 3L-NPC converter under the PD-PWM strategy can be expressed as

$$v_{j,\mathrm{PD}} = \frac{V_{dc}}{2} M \cos(\omega_0 t + \theta_j + \theta_0) + \sum_{m=1}^{\infty}\sum_{n=-\infty}^{\infty} \left[v_{hj}(2m-1, 2n) + v_{hj}(2m, 2n+1)\right] \tag{4}$$

where V_{dc} is the dc-link voltage; M is the modulation index; $\theta_j = [0, -2\pi/3, 2\pi/3]$ for $j = a, b, c$; and θ_0 is the initial phase of modulating signals. $v_{hj}(2m-1, 2n)$ denotes the odd carrier harmonic $(2m-1, 2n)$ in phase j voltage

$$v_{hj}(2m-1, 2n) = \frac{4V_{dc}}{(2m-1)\pi^2} \times \sum_{k=1}^{\infty} \frac{(2k-1)J_{2k-1}\left[(2m-1)\pi M\right]\cos(n\pi)}{(2k-1+2n)(2k-1-2n)} \times \cos\left[(2m-1)(\omega_c t + \theta_c) + 2n(\omega_0 t + \theta_j + \theta_0)\right] \tag{5}$$

while the even carrier harmonic $(2m, 2n+1)$ is expressed as

$$v_{hj}(2m, 2n+1) = \frac{V_{dc}}{2m\pi} J_{2n+1}(2m\pi M)\cos(n\pi) \times \cos\left[2m(\omega_c t + \theta_c) + (2n+1)(\omega_0 t + \theta_j + \theta_0)\right]. \tag{6}$$

Note that J_n is the Bessel function of the first kind [17]. θ_c is the initial phase of carrier signals.

According to (5) and (6), the harmonics (m, n) appearing in the phase voltage of a PD-PWM-modulated 3L-NPC converter exhibit a specific distribution pattern: odd carrier harmonics (m odd) only contain even sideband harmonics (n even), whereas even carrier harmonics (m even) only contain odd sideband harmonics (n odd). This characteristic can be named as the odd-even-coupling pattern.

For the dual NPC converter system in Fig. 2, NPC1 and NPC2 operate in a differential mode. Instead of identical modulating signals used for parallel converters, the phase j modulating signal for the xth ($x = 1, 2$) NPC converter is

$$m_{jx}(t) = M\cos(\omega_0 t + \theta_j + \theta_{0x}) \tag{7}$$

where $\theta_{01} = 0$, $\theta_{02} = \pi$, and the phase difference of π reflects the differential modulation of the dual converters.

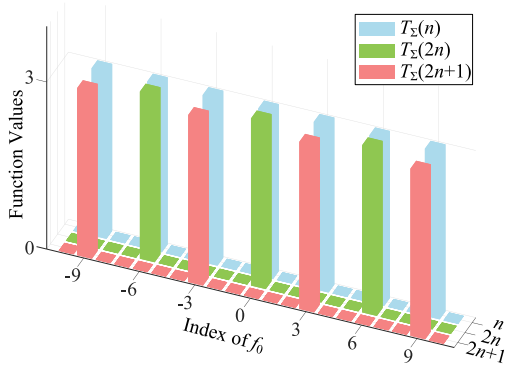

Fig. 5. 3-D plots of $T_\Sigma(n)$, $T_\Sigma(2n)$, $T_\Sigma(2n+1)$.

Based on (4) and (7), the phase j voltage of the xth converter under the PD-PWM strategy is derived as

$$v_{jx,\mathrm{PD}} = (-1)^{x+1}\frac{V_{dc}}{2} M\cos(\omega_0 t + \theta_j) + \sum_{m=1}^{\infty}\sum_{n=-\infty}^{\infty} \left[v_{hj}(2m-1, 2n) + (-1)^{x+1} v_{hj}(2m, 2n+1)\right]. \tag{8}$$

Owing to the differential modulating signals, the phase voltages of dual NPC converters have opposite fundamental and $(2m, 2n+1)$ harmonic components, while the $(2m-1, 2n)$ harmonic components remain the same between NPC1 and NPC2 because $2n$ is always an even number.

By substituting (8) into (1), the CM voltage of the xth NPC converter under the PD-PWM strategy is derived as

$$v_{\Sigma x,\mathrm{PD}} = \frac{1}{3}\sum_{m=1}^{\infty}\sum_{n=-\infty}^{\infty} \left[T_\Sigma(2n)\cdot v_{ha}(2m-1, 2n) + (-1)^{x+1} T_\Sigma(2n+1)\cdot v_{ha}(2m, 2n+1)\right] \tag{9}$$

where T_Σ, denoting the harmonic distribution term of the CM voltage, is a function of the fundamental frequency index n

$$T_\Sigma(n) = 1 + 2\cos\left(n\frac{2\pi}{3}\right). \tag{10}$$

As illustrated in Fig. 5, $T_\Sigma(n)$ is nonzero only when n is a multiple of 3, indicating that the CM voltage is composed of triplen sideband harmonics, while other harmonics are distributed in the DM voltage. The values of $T_\Sigma(2n)$ and $T_\Sigma(2n+1)$ are also plotted in Fig. 5. As indicated by these harmonic distribution terms and (9), the odd carrier harmonics in the CM voltages are located at $(2m-1, 6n)$, which are in phase between NPC1 and NPC2. In contrast, the even carrier harmonics $(2m, 6n+3)$ appear in the CM voltages with opposite phases across the dual converters.

Through substituting (9) into (2) and (3), the NL current ripple of the dual NPC converter system under the PD-PWM strategy

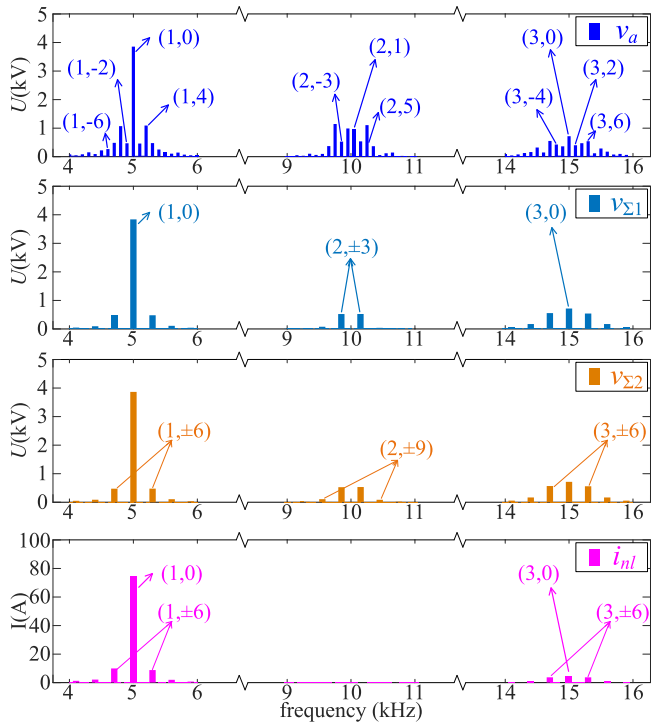

Fig. 6. Harmonic spectra of the simulated waveforms in the dual converter system under the PD-PWM strategy.

is expressed as

$$i_{nl,\mathrm{PD}} = \sum_{m=1}^{\infty}\sum_{n=-\infty}^{\infty} \frac{24V_{dc}}{\omega(L_f + L_{T2}/2)(2m-1)\pi^2} \times \sum_{k=1}^{\infty} \frac{(2k-1)J_{2k-1}\left[(2m-1)\pi M\right]\cos(n\pi)}{(2k-1+6n)(2k-1-6n)} \times \cos\left[(2m-1)(\omega_c t+\theta_c)+6n\omega_0 t\right] \quad (11)$$

where $\omega = (2m-1)\omega_c + 6n\omega_0$. According to the analytical results, the NL current ripple contains only the odd carrier harmonics $(2m-1, 6n)$, while the even carrier harmonics $(2m, 6n+3)$ are eliminated from the NL current.

To verify the theoretical analysis of harmonic distribution, the dual NPC converter system is simulated under the PD-PWM strategy, using the parameters listed in Table II. FFT is performed on the simulated phase voltage, CM voltages, and NL current, and the corresponding harmonic spectra are illustrated in Fig. 6.

As shown in the simulation results, the phase voltage v_a contains both $(2m-1, 2n)$ and $(2m, 2n+1)$ harmonics, such as $(1,-2)$ and $(2,3)$, demonstrating the odd-even-coupling pattern of the switching harmonics. For the CM voltages $v_{\Sigma1}$ and $v_{\Sigma2}$, only the $(2m-1, 6n)$ and $(2m, 6n+3)$ harmonics, such as $(1,\pm6)$ and $(2,\pm3)$, can be observed, which is consistent with the theoretical prediction in (9). Moreover, only the odd carrier harmonics $(2m-1, 6n)$ remain in the NL current i_{nl}, as the even carrier harmonics $(2m, 6n+3)$ generated by the dual converters cancel each other out.

B. Harmonic Distribution Analysis of the NL Current Ripple Under the APOD-PWM Strategy

Based on the DFSA method, the time-varying phase j ($j = a, b, c$) voltage of a 3L-NPC converter under the APOD-PWM strategy can be written as

$$v_{j,\mathrm{APOD}} = \frac{V_{dc}}{2} M\cos(\omega_0 t + \theta_j + \theta_0) + \sum_{m=1}^{\infty}\sum_{n=-\infty}^{\infty} v_{hj}(m, 2n+1) \quad (12)$$

where $v_{hj}(m, 2n+1)$ represents the harmonic $(m, 2n+1)$ of the phase j voltage

$$v_{hj}(m, 2n+1) = \frac{V_{dc}}{m\pi} J_{2n+1}(m\pi M)\cos(n\pi) \times \cos\left[m(\omega_c t+\theta_c) + (2n+1)(\omega_0 t+\theta_j+\theta_0)\right]. \quad (13)$$

According to (13), for the harmonics (m, n) generated in the phase voltage of an APOD-PWM-modulated 3L-NPC converter, only odd sideband harmonics (n odd) appear around all carrier harmonics (no matter m odd or m even). This harmonic distribution characteristic can be referred to as the odd-sideband pattern.

Based on (7) and (12), the phase j voltage of the xth NPC converter under the APOD-PWM strategy is derived as

$$v_{jx,\mathrm{APOD}} = (-1)^{x+1}\frac{V_{dc}}{2} M\cos(\omega_0 t+\theta_j) + (-1)^{x+1}\sum_{m=1}^{\infty}\sum_{n=-\infty}^{\infty} v_{hj}(m, 2n+1). \quad (14)$$

It can be concluded that all components of the phase voltage, including the fundamental and $(m, 2n+1)$ harmonic components, are opposite between the dual converters, as a consequence of differential modulating signals.

By substituting (14) into (1), the CM voltage of the xth converter under the APOD-PWM strategy is derived as

$$v_{\Sigma x,\mathrm{APOD}} = (-1)^{x+1}\sum_{m=1}^{\infty}\sum_{n=-\infty}^{\infty} \frac{V_{dc}}{m\pi} J_{6n+3}(m\pi M) \times \cos\left[(n+1)\pi\right]\cos\left[m\omega_c t + (6n+3)\omega_0 t\right]. \quad (15)$$

As indicated by (15), the CM voltages are free of the fundamental component, retaining only the harmonics $(m, 6n+3)$, which are in perfect phase opposition between the dual NPC converters.

Through substituting (15) into (2) and (3), the NL current ripple of the dual NPC converter system under the APOD-PWM strategy is expressed as

$$i_{nl,\mathrm{APOD}} = 0 \quad (16)$$

which suggests that high-order harmonics from the dual converters cancel each other out, theoretically resulting in a ripple-free NL current. However, it is worth noting that low-order harmonics, though relatively small and often negligible, may still introduce minor NL current ripple in practice.

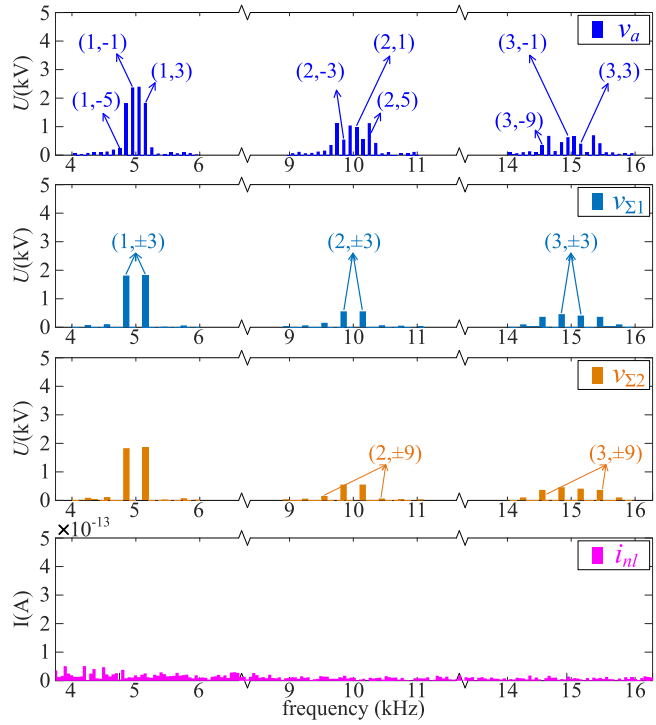

Fig. 7. Harmonic spectra of the simulated waveforms in the dual converter system under the APOD-PWM strategy.

To verify the above theoretical analysis of harmonic distribution, the dual NPC converter system in Fig. 2 is simulated under the APOD-PWM strategy, with parameters listed in Table II. The FFT analysis results of the simulated phase voltage, CM voltages, and NL current are illustrated in Fig. 7.

From the harmonic spectrum, the phase voltage v_a contains only harmonics $(m, 2n+1)$, such as $(1,-3)$ and $(2,1)$, exhibiting the odd-sideband pattern of the switching harmonic distribution. For the CM voltages $v_{\Sigma1}$ and $v_{\Sigma2}$, only harmonics $(m, 6n+3)$ appear, such as $(1,\pm3)$ and $(2,\pm9)$, which corresponds to (15). These harmonics in $v_{\Sigma1}$ and $v_{\Sigma2}$ are in phase opposition and thus cancel each other out in the NL current i_{nl}. As a consequence, no significant high-order harmonics are observed in the simulated i_{nl}.

In summary, this section has established closed-form expressions for the NL current ripple under both PD-PWM and APOD-PWM strategies, which have been consistently verified by the simulation results presented alongside the theoretical analysis. These consistent results demonstrate that the theoretical derivations accurately capture the practical ripple characteristics in the converter system and are further validated by the experimental results given in Section V.

IV. Proposed PD-TDoF Strategy for the NL Current Ripple Mitigation

Based on the previous analysis and simulation results, the dual NPC converter system in Fig. 2 exhibits significant NL current ripple when NPC1 and NPC2 are modulated using the PD-PWM strategy. In contrast, the APOD-PWM strategy produces a much smoother NL current with negligible switching

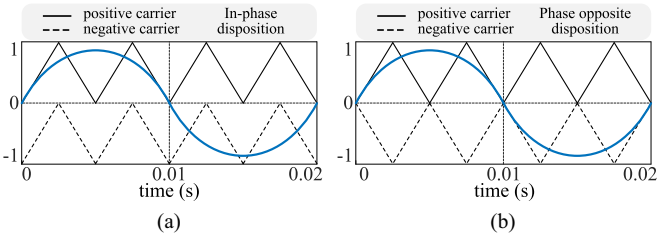

Fig. 8. Carrier configurations for three-level carrier-based PWM. (a) PD-PWM. (b) APOD-PWM.

harmonics, benefiting from the differential operating principle of the dual converters. Nevertheless, improving the performance of the PD-PWM strategy remains valuable, as it offers unique advantages in practical applications, such as superior line-to-line voltage quality [35]. To address the NL current ripple issue under the PD-PWM framework, introducing additional modulation degrees-of-freedom (DoFs) is a natural choice. This is motivated by the observation that the NL current ripple arises from imperfect harmonic cancellation between the two converters. By tuning various parameters during the modulation process, the harmonic distribution of the NL current can be manipulated, and potential ripple reduction can be achieved.

A. Discussion of Modulation Degrees-of-Freedom

In three-level carrier-based PWM, two carriers are employed for each phase. Depending on the phase relationship between two level-shifted carriers, the PD-PWM and APOD-PWM strategies can be classified, as illustrated in Fig. 8. Specifically, PD-PWM uses two carriers with identical phases, whereas APOD-PWM utilizes two phase-opposite carriers. The PD between the two carriers provides DoF1 for the modulation, resulting in different harmonic characteristics in the phase voltages, e.g., an odd-even-coupling pattern under PD-PWM and an odd-sideband harmonic pattern under APOD-PWM.

In a three-phase converter, the carriers for all three phases are generally in phase. To redistribute harmonics between the CM and DM domains, the carrier-phase-shifting (CPS) strategy adds phase shifts among the three-phase carriers, thereby introducing DoF2 in the modulation. Specific phase-shifting angles (e.g., $\theta_{ps} = 2\pi/3$) have been shown to effectively reduce the CM voltages and currents [36].

Apart from the two DoFs available in a single 3L-NPC converter, an additional DoF arises in the case of multiple converters. As a common practice to improve the output current quality of parallel converters, the interleaving strategy imposes phase shifts among the carriers of different converters, providing the DoF3. For N parallel converters, an interleaving angle of $\theta_{\text{int}} = 2\pi/N$ is typically employed [24].

The above three DoFs are all derived from the manipulation of carrier signals, while modulating signals also play a critical role in carrier-based PWM. Identical modulating signals are typically adopted for parallel converter systems, leaving no additional freedom for further harmonic shaping. However, in NL-based dc distribution systems, multiple converters are connected differently than a simple parallel configuration due to the use of dedicated transformers, e.g., the center-tapped transformer

TABLE III
SUMMARY AND COMPARISON OF FOUR DOFS

DoF	Strategy	Signal	Scope
DoF1	PD or APOD	Level-shifted carrier signals	Same phase within a converter
DoF2	Carrier phase-shifting	Three-phase carrier signals	Three phases within a converter
DoF3	Interleaving	Carriers for different converters	Multiple converters
DoF4	Differential modulation	Modulating signals	Dual converters

in Fig. 2. Differential modulating signals with a phase shift of $\theta_{\text{diff}} = \pi$ are employed between the dual NPC converters, introducing the DoF4 for modulation design.

Based on the discussion above, four DoFs have been identified for the modulation process of the dual NPC converter system. Their corresponding strategies, signals, and applicable scopes are summarized and compared in Table III for better clarity. These DoFs not only provide a framework for interpreting conventional PWM strategies but also serve as a foundation for the development of novel modulation techniques.

As demonstrated in previous analyses, the APOD-PWM strategy can effectively eliminate switching harmonics in the CM domain and achieve a ripple-free NL current. These benefits are enabled by the combined effects of DoF1 (phase-opposite carriers generating the odd-sideband harmonic pattern) and the DoF4 (differential modulating signals causing the cancellation of odd sideband harmonics between the dual converters). In contrast, under the PD-PWM strategy, only the harmonics characterized by even carrier orders and odd sidebands (m even, n odd) are eliminated from the CM domain, which is solely attributed to the use of the fourth DoF. However, harmonics with odd carrier orders and even sidebands (m odd, n even) remain in the CM domain, leading to significant NL current ripple. To address this issue, an improved PD-PWM strategy based on triple degrees-of-freedom (PD-TDoF) is proposed for the dual NPC converter system. Note that while four DoFs are defined, the first DoF is fixed by adopting PD-PWM as the baseline. The term TDoF refers to the three additional and tunable DoFs incorporated to improve system performance within this PD framework. By leveraging the three DoFs provided by the CPS, interleaving, and differential modulation strategies, the proposed PD-TDoF is capable of fully eliminating switching harmonics in the CM domain and significantly improving the NL current quality. The following analysis will explain the underlying mechanisms and demonstrate the expected improvements.

B. Harmonic Distribution Analysis of the NL Current Ripple Under the PD-TDoF Strategy

The carrier and modulating signals of the PD-TDoF strategy are illustrated in Fig. 9. Like PD-PWM, PD-TDoF employs two in-phase level-shifted carriers per phase for each converter, thereby retaining the odd-even-coupling harmonic pattern in the phase voltages, as defined in (4)–(6). However, by introducing triple DoFs, the PD-TDoF strategy applies specific phase shifts

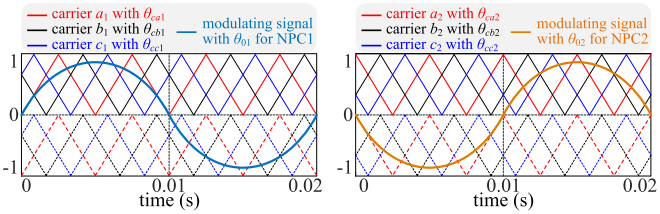

Fig. 9. Carrier and modulating signals of the proposed PD-TDoF strategy.

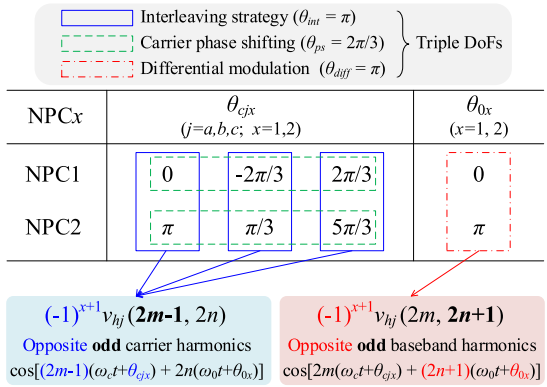

Fig. 10. Initial phases of carrier and modulating signals in the proposed PD-TDoF strategy.

to both the carrier and modulating signals, altering the harmonic distribution across the dual NPC converters. Specifically, the initial phase of the phase j ($j = a, b, c$) carrier in the xth ($x = 1, 2$) converter is shifted from θ_c to θ_{cjx} due to the CPS and interleaving strategies. Likewise, the initial phase of the modulating signals for the xth converter is shifted from θ_0 to θ_{0x} as a result of differential modulation scheme. The values of θ_{cjx} and θ_{0x} are detailed in Fig. 10.

After incorporating the phase shifts from triple DoFs into (4), the phase j voltage of xth converter under the PD-TDOF strategy is derived as

$$\begin{aligned} v_{jx,\text{TDoF}} = {} & (-1)^{x+1}\frac{V_{dc}}{2}M\cos(\omega_0 t + \theta_j) \\ & + (-1)^{x+1}\sum_{m=1}^{\infty}\sum_{n=-\infty}^{\infty} v_{hj}(2m-1, 2n) \\ & + (-1)^{x+1}\sum_{m=1}^{\infty}\sum_{n=-\infty}^{\infty} v_{hj}(2m, 2n+1). \end{aligned} \tag{17}$$

It can be observed that all phase voltage components exhibit opposite polarity between NPC1 and NPC2, which can be explained as follows with reference to Fig. 10.

1) The interleaving strategy effectively eliminates odd carrier harmonics, i.e., $(2m-1, 2n)$ in (17). By setting the interleaving angle to $\theta_{\text{int}} = \pi$, the carrier signals in NPC2 are phase-shifted by π relative to those in NPC1, resulting in phase opposition of the corresponding harmonics. Consequently, these harmonics are canceled in the NL current.
2) The differential modulation targets the elimination of odd baseband harmonics, i.e., $(2m, 2n+1)$ in (17). A phase shift of $\theta_{diff} = \pi$ between the modulating signals

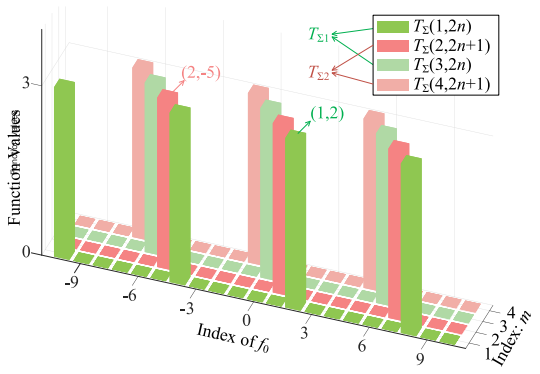

Fig. 11. 3-D plots of $T_{\Sigma1}$ and $T_{\Sigma2}$.

of NPC1 and NPC2 causes these harmonics to become phase-opposite, thereby achieving their cancellation in the NL current.

3) The CPS strategy modifies the harmonic distribution between the CM and DM domains. As will be detailed later, a carrier phase-shifting angle $\theta_{ps} = 2\pi/3$ redistributes certain dominant harmonics away from the CM domain, leading to reduced CM voltage and current.

By substituting (17) into (1), the CM voltage of the xth NPC converter under the PD-TDoF strategy is derived as

$$v_{\Sigma x,\text{TDoF}} = \frac{1}{3}\sum_{m=1}^{\infty}\sum_{n=-\infty}^{\infty}\left[(-1)^{x+1}T_{\Sigma1}\cdot v_{ha}(2m-1,2n) + (-1)^{x+1}T_{\Sigma2}\cdot v_{ha}(2m,2n+1)\right] \quad (18)$$

where $T_{\Sigma1}$ and $T_{\Sigma2}$ denote the CM harmonic distribution terms of harmonics $(2m-1,2n)$ and $(2m,2n+1)$, respectively. Their expressions are given below for the carrier phases θ_{cjx} shown in Fig. 10

$$T_{\Sigma1} = T_\Sigma(2m-1,2n) = 1+2\cos\left[(2m-1+2n)\frac{2\pi}{3}\right] \quad (19)$$

$$T_{\Sigma2} = T_\Sigma(2m,2n+1) = 1+2\cos\left[(2m+2n+1)\frac{2\pi}{3}\right]. \quad (20)$$

By comparing (9) and (18), it can be concluded that the CPS strategy exclusively modifies the CM harmonic distribution terms. Unlike the original one-variable function in (10), the new CM terms $T_{\Sigma1}$ and $T_{\Sigma2}$ are functions of two variables (m and n). Their values are visualized in Fig. 11. As can be inferred from the figure, under the PD-TDoF strategy, the odd carrier harmonics are relocated to $(2m-1, 6n-2m-2)$, while the even carrier harmonics are shifted to $(2m, 6n-2m-3)$. Both of them are opposite between the CM voltages of NPC1 and NPC2, as indicated in (18).

By substituting (18) into (2) and (3), the NL current ripple of the dual NPC converter system under the proposed PD-TDoF strategy is expressed as

$$i_{nl,\text{TDoF}} = 0 \quad (21)$$

which suggests that all high-order harmonics from the dual converters mutually cancel out, theoretically eliminating the NL current ripple. However, low-order harmonics, while typically small and often negligible, may still induce a minor residual ripple in practical applications.

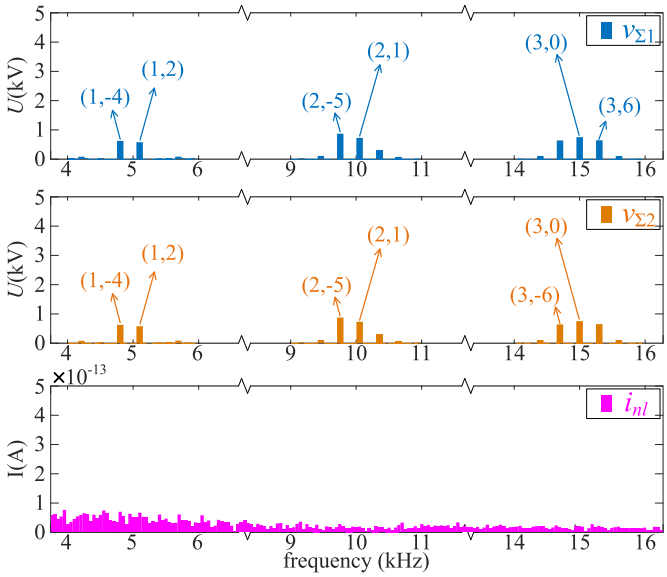

Fig. 12. Harmonic spectra of the simulated waveforms in the dual converter system under the proposed PD-TDoF strategy.

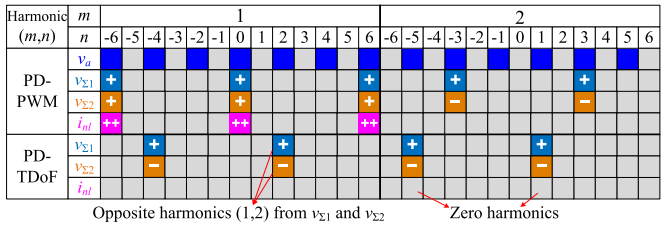

Fig. 13. Harmonic distributions under the PD-PWM and PD-TDoF strategies.

To validate the theoretical analysis of harmonic distribution, the dual NPC converter system shown in Fig. 2 is simulated under the proposed PD-TDoF strategy using the parameters listed in Table II. The FFT analysis results of the simulated CM voltages and NL current are depicted in Fig. 12.

Compared to the previous results in Fig. 6, the simulated CM voltages under the PD-TDoF strategy exhibit switching harmonics of different orders. Specifically, the PD-PWM strategy produces CM harmonics at $(1,0)$ and $(1,\pm6)$, whereas the PD-TDoF shifts them to $(1,-4)$ and $(1,2)$. Notably, the elimination of the dominant $(1,0)$ harmonic in the CM domain can suppress CM currents in the dual converters, contributing to reduced size of CM choke and improved power density of converters. Moreover, all the harmonics in $v_{\Sigma1}$ and $v_{\Sigma2}$ are phase-opposed, leading to their cancellation in i_{nl}. As a result, the simulated i_{nl} exhibits no significant high-order harmonics.

C. Comparative Analysis of PD-PWM and the Proposed PD-TDoF Strategies

To compare the performance of the PD-PWM and proposed PD-TDoF strategies, Fig. 13 provides an illustration of their

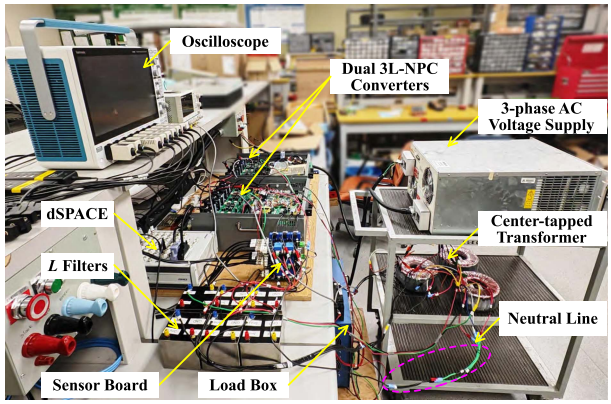

Fig. 14. Photograph of the experimental setup.

respective harmonic distributions. Note that the symbols "+" and "−" indicate the relative polarities of the harmonics, rather than the sign of their magnitudes.

The phase voltages under both strategies exhibit identical harmonic distributions, where v_a contains both $(2m-1, 2n)$ and $(2m, 2n+1)$ harmonics, reflecting the same odd-even-coupling pattern of the switching harmonic distribution.

In terms of harmonic characteristics in the CM voltages and NL current, Fig. 13 shows that the conventional PD-PWM strategy generates in-phase odd carrier harmonics $(2m-1, 6n)$ in $v_{\Sigma 1}$ and $v_{\Sigma 2}$, while introducing out-of-phase even carrier harmonics $(2m, 6n+3)$ in the CM domain through differential modulation. Consequently, i_{nl} accumulates $(2m-1, 6n)$ harmonics while canceling $(2m, 6n+3)$ components.

In contrast, the proposed PD-TDoF strategy provides three DoFs that fundamentally reconfigure harmonic distributions in CM voltages and NL current. 1) The CPS strategy shifts the odd carrier harmonics to $(2m-1, 6n-2m-2)$ and the even carrier harmonics to $(2m, 6n-2m-3)$. 2) The interleaving strategy introduces a DoF that ensures opposite harmonics $(2m-1, 6n-2m-2)$ between $v_{\Sigma 1}$ and $v_{\Sigma 2}$; 3) The differential modulation generates anti-phase $(2m, 6n-2m-3)$ harmonics in the two CM voltages. As a result, this coordinated modulation strategy enables complete cancellation of both odd and even carrier harmonics in i_{nl}, achieving improved NL current performance compared to conventional PD-PWM.

V. Experimental Verification

To verify the theoretical analysis and evaluate the effectiveness of the proposed PD-TDoF modulation strategy for the dual NPC converter system, laboratory experiments were carried out. The experimental setup is shown in Fig. 14. A three-phase programmable ac power supply is used to emulate the ac grid. Two 3L-NPC converters are connected to the ac power supply through a center-tapped transformer, with their dc sides feeding a resistive load bank. The PWM strategies studied in this article are implemented using the dSPACE MicroLabBox DS1202. The experimental parameters are listed in Table IV.

TABLE IV
Experimental System Parameters

Parameter	Value	Parameter	Value
Grid RMS line voltage	208 V	DC-link voltage	200 V
Grid frequency	50 Hz	Switching frequency	5 kHz
Transformer turns ratio	2.18 : 1 : 1	Capacitance per pole	580 μF
Filter inductance (L_f)	3 mH	DC loads (R_p, R_n)	28.8 Ω

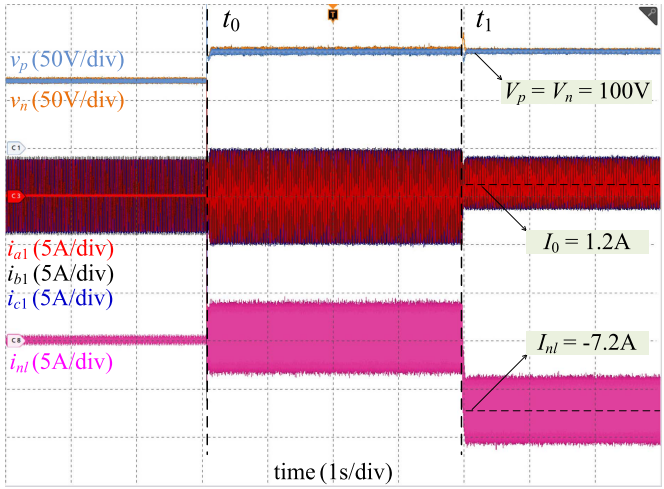

Fig. 15. Experimental waveforms illustrating the DC-side voltage balancing and NL current ripple issue.

A. Experimental Results Under the PD-PWM Strategy

Fig. 15 illustrates the operating principles and key challenges of the dual NPC converter system. Initially, the converters function in an uncontrolled rectification mode. At t_0, PD-PWM is enabled for both converters, and the control strategy regulates the dc-link voltage at $v_{dc} = 200\,V$. Under balanced load conditions, no dc balancing current is required, resulting in a zero dc component in the NL current i_{nl}. At t_1, the negative load R_n is disconnected, and the dc loads become extremely unbalanced. Despite this, the pole voltages v_p and v_n remain stable at $100\,V$, demonstrating the full bipolar voltage balancing capability of the system. Due to the reduced load power, the ac current amplitudes of NPC1 and NPC2 (i_{abc1} and i_{abc2}) are halved, and zero-sequence components appear in both. In this NL-based system, the dc currents through the converters ($I_0 = 1.2$ A) and the NL ($I_{nl} = -6I_0 = -7.2$ A) are critical for keeping dc-side voltage balance. However, significant current ripple is observed in i_{nl} under both balanced and unbalanced load conditions, posing power quality challenges and leading to adverse effects such as overheating or even failure of the NL wiring.

To further illustrate the NL current ripple issue in the dual NPC converter system, the experimental CM currents ($i_{\Sigma 1}$, $i_{\Sigma 2}$) and the NL current (i_{nl}) waveforms, zoomed around t_1, are presented in Fig. 16. Throughout the entire operation, both the useful dc components and undesired ripples in $i_{\Sigma 1}$ and $i_{\Sigma 2}$ accumulate in i_{nl}, as described by (3). The peak-to-peak ripple of i_{nl} measures 6.3 A, corresponding to 1.82 p.u. relative to the dc load current

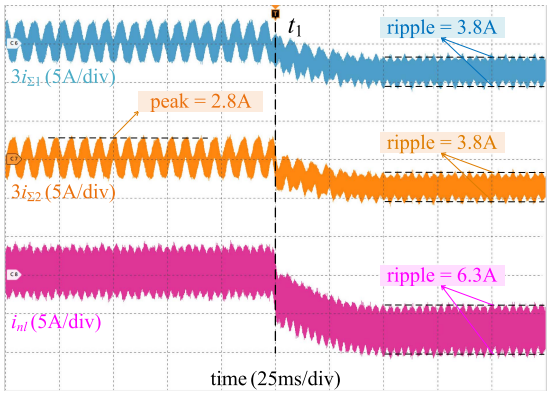

Fig. 16. Experimental waveforms of the CM currents and NL current under the PD-PWM strategy.

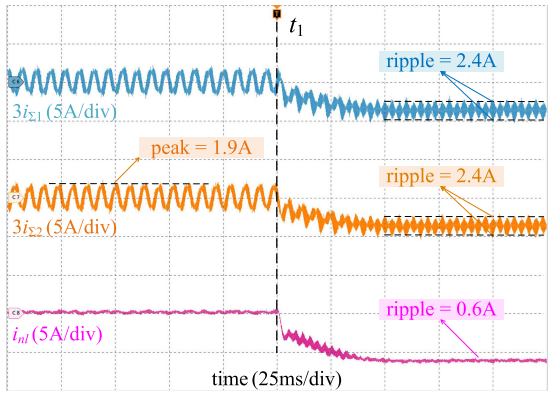

Fig. 18. Experimental waveforms of the CM currents and NL current under the APOD-PWM strategy.

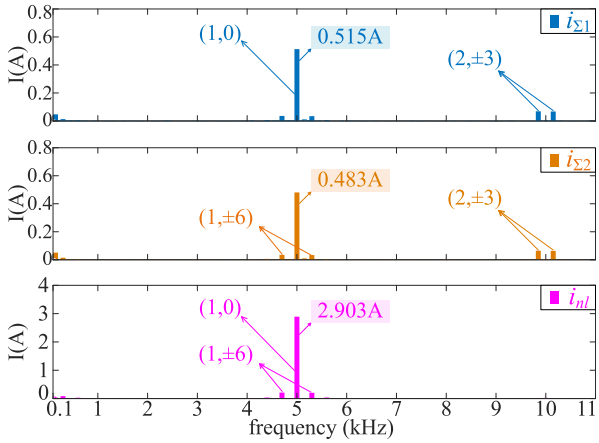

Fig. 17. Harmonic spectra of the experimental $i_{\Sigma1}$, $i_{\Sigma2}$, and i_{nl} under the PD-PWM strategy.

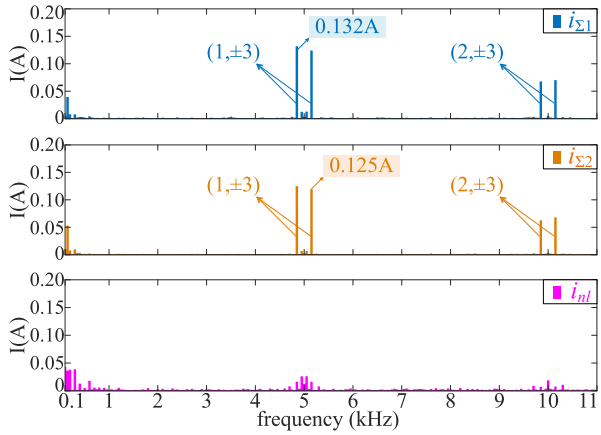

Fig. 19. Harmonic spectra of the experimental $i_{\Sigma1}$, $i_{\Sigma2}$, and i_{nl} under the APOD-PWM strategy.

($I_{dc} = V_{dc}/2R_p = 3.47$ A). This substantial ripple highlights the necessity of effective ripple mitigation.

FFT analysis is implemented for further clarifying the harmonic components in the currents, and the results are shown in Fig. 17. The odd carrier harmonics (1,0) and $(1, \pm 6)$ are observed in all three currents. These components are in-phase between $i_{\Sigma1}$ and $i_{\Sigma2}$, and thus accumulate in i_{nl}, which corresponds to (11). In contrast, harmonics $(2, \pm 3)$ appear in both $i_{\Sigma1}$ and $i_{\Sigma2}$ but are absent in i_{nl}, validating their out-of-phase characteristics as indicated by (9). The cancellation of even carrier harmonics contributes to a partial ripple reduction in i_{nl}. Nevertheless, the NL current ripple is still very large due to the dominant harmonic (1,0), which has an amplitude of 2.903 A. The experimental results are consistent with the theoretical analysis presented in Section III-A.

B. Experimental Results Under the APOD-PWM Strategy

The performance of the APOD-PWM strategy in the dual converter system is experimentally validated. Fig. 18 displays the experimental waveforms of the CM currents and NL current captured around t_1. High-frequency ripple is observed in $i_{\Sigma1}$ and $i_{\Sigma2}$ under both balanced and unbalanced load conditions. During unbalanced operation, low-order harmonics also appear due to the presence of zero-sequence currents [31]. The ripple amplitudes in $i_{\Sigma1}$ and $i_{\Sigma2}$ are lower than those shown in Fig. 16. Moreover, the NL current ripple is even smaller than the CM current ripple, indicating partial ripple cancellation between the dual converters. Compared to i_{nl} under the PD-PWM strategy, APOD-PWM achieves a significantly smoother NL current waveform.

To further investigate the ripple reduction achieved by APOD-PWM, Fig. 19 presents the FFT analysis results of the CM currents and NL current. The dominant harmonic components in $i_{\Sigma1}$ and $i_{\Sigma2}$ are limited to $(1, \pm 3)$ and $(2, \pm 3)$, which aligns with the theoretical prediction in (15). No significant high-order harmonics are observed in i_{nl}, as the harmonics in $i_{\Sigma1}$ and $i_{\Sigma2}$ exhibit out-of-phase characteristics, leading to mutual cancellation in i_{nl}. Consequently, the high-frequency ripple of i_{nl} is reduced to nearly zero, validating the analytical prediction of (16). A residual NL current ripple remains, however, attributed to low-order harmonics and unbalanced high-order harmonics.

C. Experimental Results of the Proposed PD-TDoF Strategy

The effectiveness and advantages of the proposed PD-TDoF strategy are validated through experimental results. Fig. 20 displays the experimental waveforms of the CM currents and

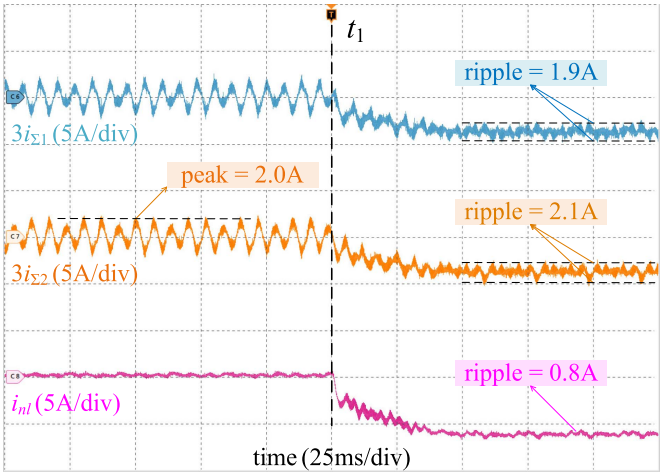

Fig. 20. Experimental waveforms of the CM currents and NL current under the proposed PD-TDoF strategy.

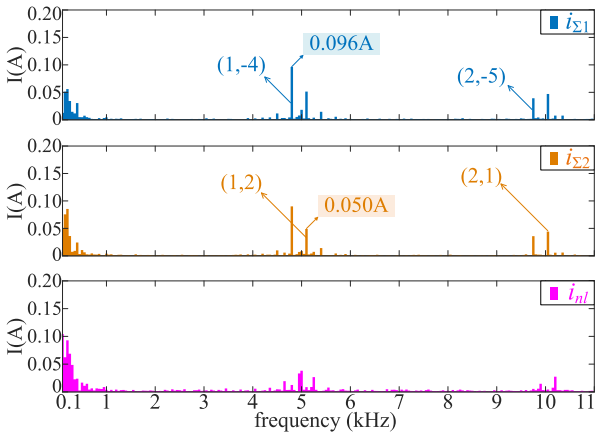

Fig. 21. Harmonic spectra of the experimental $i_{\Sigma1}$, $i_{\Sigma2}$, and i_{nl} under the proposed PD-TDoF strategy.

NL current recorded around t_1. High-frequency ripple is present in $i_{\Sigma1}$ and $i_{\Sigma2}$ throughout the entire operation. Compared to the PD-PWM strategy, the proposed PD-TDoF strategy effectively reduces the peak amplitudes of the CM currents. For instance, during balanced operation ($t < t_1$), the peak value of $i_{\Sigma2}$ under PD-TDoF is measured as $2.0/3 = 0.67$ A, representing a 28% reduction compared to PD-PWM ($2.8/3 = 0.93$ A, as shown in Fig. 16). In addition, the proposed PD-TDoF strategy demonstrates a notable capability for ripple suppression. For unbalanced operation ($t > t_1$), the NL current ripple is mitigated from 6.3 A (PD-PWM) to 0.8 A (PD-TDoF), corresponding to an 87.3% reduction. As a result, the waveform of i_{nl} under PD-TDoF is significantly smoother than that in Fig. 16.

Fig. 21 presents the FFT analysis results of all experimental currents. Compared to the current harmonic distribution under the PD-PWM strategy (see Fig. 17), the proposed PD-TDoF strategy shifts the switching harmonic orders by virtue of the DoF introduced by the CPS strategy. Specifically, harmonics (1,0) and $(1, \pm 6)$ observed under PD-PWM are shifted to $(1, -4)$ and (1,2) under PD-TDoF. The elimination of the harmonic (1,0), along with the reduced amplitudes of the new

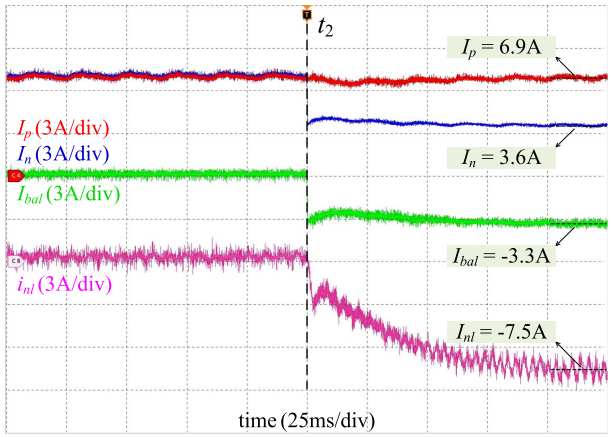

Fig. 22. DC-side experimental waveforms of the dual NPC converter system under the PD-TDoF modulation strategy.

CM harmonics, is critical to achieving lower peak values of the CM currents. Furthermore, the proposed PD-TDoF strategy effectively eliminates significant CM harmonics in i_{nl}, as all high-order harmonics are out of phase between $i_{\Sigma1}$ and $i_{\Sigma2}$ according to (18), theoretically achieving zero NL current ripple, as indicated by (21). The removal of significant harmonics in i_{nl} validates the benefits of the DoFs introduced by interleaving and differential modulation and explains the dramatic reduction in NL current ripple observed in Fig. 20. However, i_{nl} is not entirely ripple-free in practice due to residual low-order harmonics. The phase-shifted switching patterns in the PD-TDoF strategy create differential timing between phases, which imposes burden to practical implementation and causes additional low-order harmonics in i_{nl}.

The effectiveness of the proposed PD-TDoF strategy is further verified under an additional operating scenario for the dual NPC converter system. In contrast to the original scenario with $28.8\,\Omega$ dc loads and a unity power factor, the new experiment features heavier dc loads ($14.4\,\Omega$) and a lower power factor (PF $= 0.80$), representing a higher power condition with increased reactive power demand. Fig. 22 presents the measured dc-side current waveforms, where I_p, I_n, I_{bal} represent the dc components of the positive pole, negative pole, and the balancing currents, respectively; i_{nl} denotes the NL current. Initially, balanced dc loads ($R_p = R_n = 14.4\,\Omega$) are supplied, resulting in no need for a balancing current. The pole currents are equal ($I_p = I_n = 6.9$ A), and i_{nl} exhibits zero dc component. At t_2, a load imbalance is introduced as the load on the negative pole becomes lighter ($R_n = 28.8\,\Omega$). Since the active control strategy maintains pole voltage balance, the current I_n immediately drops to 3.6 A, triggering a balancing current $I_{\text{bal}} = 3.3$ A. The NL current builds up to a stable value $I_{nl} = -7.5$ A within $0.1\,s$, demonstrating the system's fast dynamic response and robust voltage balancing capability under the new load change condition. More importantly, the proposed PD-TDoF strategy continues to provide effective mitigation for most NL current ripple, even under this more challenging operating scenario.

Given that the APOD-PWM strategy is also effective in mitigating NL current ripple, the proposed PD-TDoF strategy is

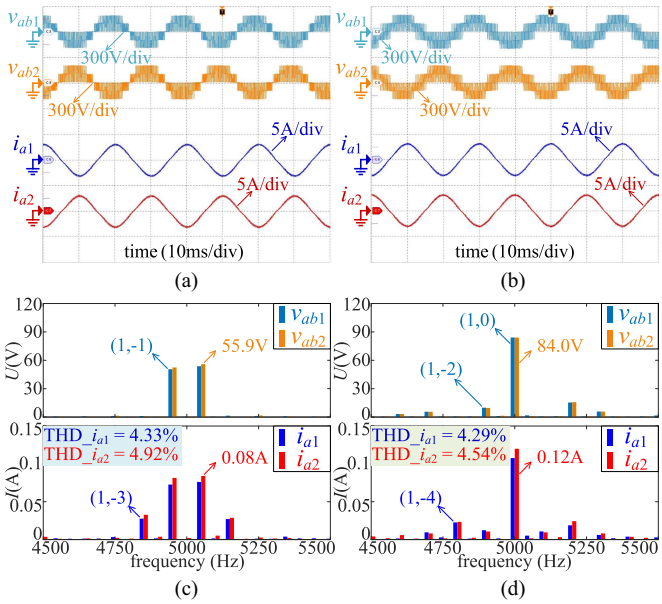

Fig. 23. AC-side experimental results under different modulation strategies. (a) Waveforms under APOD-PWM. (b) Waveforms under PD-TDoF. (c) FFT results under APOD-PWM. (d) FFT results under PD-TDoF.

compared with the conventional APOD-PWM in other metrics. The ac-side waveforms and their harmonic spectra under both strategies are presented in Fig. 23. The line-to-line switching voltages of NPC1 and NPC2 (v_{ab1} and v_{ab2}) exhibit larger and fewer voltage steps under APOD-PWM, while the proposed PD-TDoF strategy generates finer and more frequent voltage steps by distributing the switching actions over time and across phases. The ac-side phase currents (i_{a1} and i_{a2}) are nearly sinusoidal and exhibit similar waveforms under both APOD-PWM and PD-TDoF. According to the FFT results in Fig. 23(c) and (d), the total harmonic energy of the line-to-line voltages is comparable for both strategies. The proposed PD-TDoF exhibits the harmonic energy concentration characteristic, which is advantageous for practical filter design. The phase currents under APOD-PWM and PD-TDoF have different harmonic spectra around the switching frequency, which corresponds to the theoretical equations (14) and (17). However, their THD values are comparable as a result of the relatively small harmonic amplitudes.

In summary, the experimental results validate the advantages of the proposed PD-TDoF strategy in: 1) eliminating high-order switching harmonics and suppressing NL current ripple; and 2) shifting CM harmonic orders and reducing the peak values of the CM currents. Moreover, it does not increase phase current distortion or degrade the ac-side power quality.

VI. Conclusion

As a promising solution for bipolar dc distribution, NL-based 3L-NPC converter systems offer advantages in structural simplicity and cost-effectiveness compared to VB-based systems, but suffer from significant ripple in the NL current. This article presents an in-depth analysis of NL current ripple in a dual NPC converter system. By applying the DFSA method, analytical expressions are derived to characterize the switching harmonic distributions of NL current ripple under different PWM strategies.

1) Under PD-PWM, odd carrier harmonics $(2m-1, 6n)$ are in-phase between the dual converters, thus accumulating in the NL current and causing significant current ripple, while even carrier harmonics $(2m, 6n+3)$ are canceled.
2) Under APOD-PWM, only harmonics $(m, 6n+3)$ appear in the CM current, which are phase-opposite between the dual converters and therefore cancel out, resulting in a much smoother NL current.

To mitigate the large NL current ripple under the PD-PWM strategy, this article proposes a PD-TDoF modulation strategy, which leverages three DoFs to achieve multiple advantages.

1) The two DoFs introduced by interleaving and differential modulation drive both odd and even carrier harmonics out of phase between the dual converters, thus ensuring effective harmonic cancellation in the NL current and a substantial ripple reduction over conventional PD-PWM.
2) The DoF provided by CPS reshapes the CM harmonic profile and eliminates dominant harmonics from the CM domain, thereby reducing CM current peaks and allowing for more compact CM chokes and improved converter power density.

Theoretical findings are supported by simulations and validated through laboratory experiments, confirming the effectiveness and advantages of the proposed PD-TDoF strategy.

References

[1] B. Grainger and R. De Doncker, "Medium Voltage DC System Architectures," London, U.K.: Inst. Eng. Technol., 2021, Art. no. 392.
[2] T. Dragicevic, J. C. Vasquez, J. M. Guerrero, and D. Skrlec, "Advanced LVDC electrical power architectures and microgrids: A step toward a new generation of power distribution networks," *IEEE Electrif. Mag.*, vol. 2, no. 1, pp. 54–65, Mar. 2014.
[3] CIGRE WG C6/B4.37, *Medium Voltage DC Distribution Systems*, Tech. Brochure, Paris, France: CIGRE, vol. 875, 2022. [Online]. Available: https://www.e-cigre.org/publications/detail/875-medium-voltage-dcdistribution-systems.html
[4] Y. R. Li, F. Nejabatkhah, and H. Tian, *Smart Hybrid AC/DC Microgrids: Power Management, Energy Management, and Power Quality Control*. Hoboken, NJ, USA: Wiley, 2022.
[5] P. Salonen, T. Kaipia, P. Nuutinen, P. Peltoniemi, and J. Partanen, "An LVDC distribution system concept," in *Proc. NordicWorkshop Power Ind. Electron.*, 2008, pp. A3–1–A3–16.
[6] S. Rivera, R. Lizana, S. Kouro, and B. Wu, "Bipolar-type DC microgrids for high-quality power distribution," in *DC Distrib. Syst. and Microgrids*, London, U.K.: Inst. Eng. Technol., 2018, pp. 245–266.
[7] R. Teichmann and S. Bernet, "A comparison of three-level converters versus two-level converters for low-voltage drives, traction, and utility applications," *IEEE Trans. Ind. Appl.*, vol. 41, no. 3, pp. 855–865, May–Jun. 2005.
[8] J. Chen, W. Ming, C. E. Ugalde-Loo, S. Wang, and N. Jenkins, "Analysis and mitigation of DC voltage imbalance for medium-voltage cascaded three-level neutral-point-clamped converters," *IEEE Trans. Power Electron.*, vol. 37, no. 4, pp. 4320–4336, Apr. 2022.
[9] J. Yu, K. Smith, M. Urizarbarrena, N. MacLeod, R. Bryans, and A. Moon, "Initial designs for the ANGLE DC project; converting existing AC cable and overhead line into DC operation," in *Proc. 13th IET Int. Conf. AC DC Power Transmiss.*, 2017, pp. 1–6.
[10] S. Rivera, B. Wu, S. Kouro, V. Yaramasu, and J. Wang, "Electric vehicle charging station using a neutral point clamped converter with bipolar DC bus," *IEEE Trans. Ind. Electron.*, vol. 62, no. 4, pp. 1999–2009, Apr. 2015.

[11] B. Li, H. Tian, L. Ding, X. Wu, G. J. Kish, and Y. R. Li, "An improved three-level neutral point clamped converter system with full-voltage balancing capability for bipolar low-voltage DC grid," *IEEE Trans. Power Electron.*, vol. 38, no. 12, pp. 15792–15803, Dec. 2023.
[12] H. Kakigano, Y. Miura, and T. Ise, "Low-voltage bipolar-type DC microgrid for super high quality distribution," *IEEE Trans. Power Electron.*, vol. 25, no. 12, pp. 3066–3075, Dec. 2010.
[13] F. Wang, Z. Lei, X. Xu, and X. Shu, "Topology deduction and analysis of voltage balancers for DC microgrid," *IEEE J. Emerg. Sel. Top. Power Electron.*, vol. 5, no. 2, pp. 672–680, Jun. 2017.
[14] S. Rivera, R. Lizana F., S. Kouro, T. Dragičević, and B. Wu, "Bipolar dc power conversion: State-of-the-art and emerging technologies," *IEEE J. Emerg. Sel. Top. Power Electron.*, vol. 9, no. 2, pp. 1192–1204, Apr. 2021.
[15] V. F. Pires, A. Cordeiro, C. Roncero-Clemente, S. Rivera, and T. Dragičević, "DC–DC converters for bipolar microgrid voltage balancing: A comprehensive review of architectures and topologies," *IEEE J. Emerg. Sel. Top. Power Electron.*, vol. 11, no. 1, pp. 981–998, Feb. 2023.
[16] C. Perera, J. Salmon, and G. J. Kish, "Multiport converter with independent control of AC and DC power flows for bipolar DC distribution," *IEEE Trans. Power Electron.*, vol. 36, no. 3, pp. 3473–3485, Mar. 2020.
[17] D. G. Holmes and T. A. Lipo, *Pulse Width Modulation for Power Converters: Principles and Practice*. Hoboken, NJ, USA: Wiley, 2003.
[18] P. Rodriguez, J. I. Candela, A. Luna, L. Asiminoaei, R. Teodorescu, and F. Blaabjerg, "Current harmonics cancellation in three-phase four-wire systems by using a four-branch star filtering topology," *IEEE Trans. Power Electron.*, vol. 24, no. 8, pp. 1939–1950, Aug. 2009.
[19] H.-L. Jou, J.-C. Wu, K.-D. Wu, W.-J. Chiang, and Y.-H. Chen, "Analysis of zig-zag transformer applying in the three-phase four-wire distribution power system," *IEEE Trans. Power Del.*, vol. 20, no. 2, pp. 1168–1173, Apr. 2005.
[20] G. Escobar, A. A. Valdez, R. E. Torres-Olguin, and M. F. Martinez-Montejano, "A model-based controller for a three-phase four-wire shunt active filter with compensation of the neutral line current," *IEEE Trans. Power Electron.*, vol. 22, no. 6, pp. 2261–2270, Nov. 2007.
[21] O. Vodyakho and C. C. Mi, "Three-level inverter-based shunt active power filter in three-phase three-wire and four-wire systems," *IEEE Trans. Power Electron.*, vol. 24, no. 5, pp. 1350–1363, May 2009.
[22] S. Choi and M. Jang, "Analysis and control of a single-phase-inverter–zigzag-transformer hybrid neutral-current suppressor in three-phase four-wire systems," *IEEE Trans. Ind. Electron.*, vol. 54, no. 4, pp. 2201–2208, Aug. 2007.
[23] Z.-X. Zou, F. Hahn, G. Buticchi, S. Günter, and M. Liserre, "Interleaved operation of two neutral-point-clamped inverters with reduced circulating current," *IEEE Trans. Power Electron.*, vol. 33, no. 12, pp. 10122–10134, Dec. 2018.
[24] Z. Quan and Y. W. Li, "Suppressing zero-sequence circulating current of modular interleaved three-phase converters using carrier phase shift PWM," *IEEE Trans. Ind. Appl.*, vol. 53, no. 4, pp. 3782–3792, Jul.–Aug. 2017.
[25] A. Tcai, Y. Kwon, S. Pugliese, and M. Liserre, "Reduction of the circulating current among parallel NPC inverters," *IEEE Trans. Power Electron.*, vol. 36, no. 11, pp. 12504–12514, Nov. 2021.
[26] W. Li et al., "Integrated modulation of dual-parallel three-level inverters with reduced common mode voltage and circulating current," *IEEE Trans. Power Electron.*, vol. 36, no. 11, pp. 13332–13344, Nov. 2021.
[27] P. Zhang et al., "Integration modulation for current ripple and high-frequency zero-sequence circulating current reduction on two-parallel three-level converters," *IEEE Trans. Ind. Electron.*, vol. 71, no. 8, pp. 8216–8226, Aug. 2024.
[28] *Recommended Practice for Establishing Transformer Capability When Supplying Nonsinusoidal Load Currents*, IEEE Standard C57.110-1998, 1999, pp. 1–48. [Online]. Available: https://www.en-standard.eu/ieee-c57-110-1986-ieee-recommended-practice-for-establishing-transformer-capability-whensupplying-nonsinusoidal-load-currents-2/
[29] T. M. Gruzs, "A survey of neutral currents in three-phase computer power systems," *IEEE Trans. Ind. Appl.*, vol. 26, no. 4, pp. 719–725, Jul.–Aug. 1990.
[30] D. Sreenivasarao, P. Agarwal, and B. Das, "Neutral current compensation in three-phase, four-wire systems: A review," *Elect. Power Syst. Res.*, vol. 86, pp. 170–180, 2012.
[31] B. Li, X. Wu, G. J. Kish, and Y. R. Li, "Dual 3L-NPC converter system with improved power quality for bipolar DC distribution," *IEEE Trans. Power Electron.*, vol. 39, no. 12, pp. 16553–16565, Dec. 2024.
[32] W. Bennett, "New results in the calculation of modulation products," *Bell Syst. Tech. J.*, vol. 12, no. 2, pp. 228–243, 1933.
[33] S. Bowes and B. Bird, "Novel approach to the analysis and synthesis of modulation processes in power convertors," *Proc. Inst. Electr. Eng.*, vol. 122, no. 5, pp. 507–513, 1975.
[34] J. Shen, S. Schroder, B. Duro, and R. Roesner, "A neutral-point balancing controller for a three-level inverter with full power-factor range and low distortion," *IEEE Trans. Ind. Appl.*, vol. 49, no. 1, pp. 138–148, Jan.–Feb. 2013.
[35] B. Cougo, G. Gateau, T. Meynard, M. Bobrowska-Rafal, and M. Cousineau, "PD modulation scheme for three-phase parallel multilevel inverters," *IEEE Trans. Ind. Electron.*, vol. 59, no. 2, pp. 690–700, Feb. 2012.
[36] J. W. Kimball and M. Zawodniok, "Reducing common-mode voltage in three-phase sine-triangle PWM with interleaved carriers," *IEEE Trans. Power Electron.*, vol. 26, no. 8, pp. 2229–2236, Aug. 2011.

Bowei Li (Graduate Student Member, IEEE) received the B.S. and M.S. degrees in electrical engineering from Shandong University, Jinan, China, in 2017 and 2020, respectively. He is currently working toward the Ph.D. degree in energy system with the Department of Electrical and Computer Engineering, University of Alberta, Edmonton, AB, Canada.

His research interests include topology, control, and power quality of bipolar dc distribution systems.

Gregory J. Kish (Senior Member, IEEE) received the B.E.Sc. degree from the University of Western Ontario, London, ON, Canada, in 2009, and the M.A.Sc. and Ph.D. degrees from the University of Toronto, Toronto, ON, Canada, in 2011 and 2016, respectively, all in electrical engineering.

He is currently an Associate Professor with the University of Alberta, Edmonton, AB, Canada. His research interests include the development and application of power electronic converter systems in electric grids.

Yunwei Ryan Li (Fellow, IEEE) received the B.Sc. in Engineering degree in electrical engineering from Tianjin University, Tianjin, China, in 2002, and the Ph.D. degree in electrical engineering from Nanyang Technological University, Singapore, in 2006.

In 2005, he was a Visiting Scholar with Aalborg University, Aalborg, Denmark. From 2006 to 2007, he was a Postdoctoral Research Fellow with the Toronto Metropolitan University, Canada. In 2007, he also worked with Rockwell Automation Canada before he joined the University of Alberta, Canada in the same year. He is currently a Professor, University of Alberta Senior Engineering Research Chair, and Chair of the Department of Electrical and Computer Engineering. His research interests include distributed generation, microgrid, renewable energy, high power converters and electric motor drives.

Dr. Li is the Vice President for Products of IEEE Power Electronics Society (PELS) 2022–2026. He was the Editor-in-Chief for IEEE TRANSACTIONS ON POWER ELECTRONICS LETTERS 2019–2023. He served as the general chair of IEEE Energy Conversion Congress of Exposition (ECCE) in 2020 for the first-ever virtual version during the pandemic. He received the Research Excellence Summit Award by the Association of Professional Engineers and Geoscientists of Alberta in 2025, the Nagamori Foundation Award in 2022, and the Richard M. Bass Outstanding Young Power Electronics Engineer Award from IEEE PELS in 2013. He is a Fellow of the Canadian Academy of Engineering, and recognized as the Clarivate Highly Cited Researcher.